Journal of Solid State Chemistry 183 (2010) 2522–2527

Contents lists available at ScienceDirect

Journal of Solid State Chemistry

journal homepage: www.elsevier.com/locate/jssc

Synthesis and spectroscopic characterization of P-doped Na_4Si_4

Jialing Wang [a], Sabyasachi Sen [b], Ping Yu [c], Nigel D. Browning [b], Susan M. Kauzlarich [a,*]

[a] Department of Chemistry, University of California, One Shields Avenue, Davis, CA 95616, USA
[b] Department of Chemical Engineering and Materials Science, University of California, One Shields Avenue, Davis, CA 95616, USA
[c] NMR Facility, University of California, One Shields Avenue, Davis, CA 95616, USA

ARTICLE INFO

Article history:
Received 22 July 2010
Accepted 31 July 2010
Available online 11 August 2010

Keywords:
Zintl phase
Metal silicide
Raman spectroscopy
Solid-state multinuclear NMR
Clathrate

ABSTRACT

Na_4Si_4 is a Zintl salt composed of Na^+ cations and Si_4^{4-} tetrahedral anions and is a unique solid-state precursor to clathrate structures and nanomaterials. In order to provide opportunities for the synthesis of complex materials, phosphorus was explored as a possible substituent for silicon. Phosphorus doped sodium silicides $Na_4Si_{4-x}P_x$ ($x \leq 0.04$) were prepared by reaction of Na with the mechanically alloyed Si_{4-x}:P_x (x=0.04, 0.08, 0.12) mixture in a sealed Nb tube at 650 °C for 3 days. Energy dispersive X-ray spectroscopy confirms the presence of P in all products. Powder X-ray diffraction patterns are consistent with the retention of the Na_4Si_4 crystal structure. As the amount of P increases, a new peak in the diffraction pattern that can be assigned to black phosphorus is apparent above the background. Raman and solid-state NMR provide information on phosphorus substitution in the Na_4Si_4 structure. Raman spectroscopy shows a shift of the most intense band assigned to the Si_4^{4-} ν_1 (A_1) mode from 486.4 to 484.0 cm^{-1} with increasing P, consistent with P replacement of Si. Differential nuclear spin-lattice relaxation for the Si sites determined via ^{29}Si solid-state NMR provides direct evidence for Si–P bonding in the $(Si_{1-x}P_x)^{4-}$ tetrahedron. The ^{23}Na NMR shows additional Na…P interactions and the ^{31}P NMR shows two P sites, consistent with P presence in both of the crystallographic sites in the $(Si_4)^{4-}$ tetrahedron.

1. Introduction

Metal silicides have long been of great interest to the silicon-based integration technology [1]. Among them only a few are semiconducting silicides, which are mainly made from metals in groups 2 (Mg and Ba only), 6, 7, and 8 of the Periodic Table. In contrast, group 1 alkali metal silicides are not identified as semiconducting silicides. Like the group 2 alkaline earth metal silicides, the alkali metal silicides are known as Zintl phases, but have quite different structures and properties from the former. Na_4Si_4 is used as a precursor to inorganic clathrate phases [2–6]. These phases have the compositions Na_8Si_{46} and Na_xSi_{136} and have been explored for possible thermoelectric applications [7,8]. With the Na removed, they are of interest as wide band gap semiconductors [9]. It was not until recent years that NaSi or Na_4Si_4 (written as such to draw attention to the Si_4 cluster in the solid), an alkali metal silicide, was found to be an excellent precursor for synthesis of Si nanoparticles (NPs) via reaction with silicon halides [10], ammonium halides [11–13], or via direct ultrasonication [14]. It thus provides a unique reagent for the preparation of nanocrystalline Si material for thin-film microelectronics or optoelectronics such as solar cells. The advantages include low temperature and ambient pressure route, easy manipulation of the Si NP's surface and potential for large scale manufacturing.

Intentional impurity doping has been a traditional approach to enhance the desirable material properties for both semiconducting silicides, resulting in "ternary silicides" [15,16], and Si NPs [17–23]. In these applications P is of paramount importance as an *n*-type dopant [17]. There are a variety of techniques to dope impurity atoms into the substrate materials, such as spark plasma sintering [15], plasma-enhanced chemical vapor deposition [24], ion implantation followed by thermal annealing [25], reactive radio-frequency co-sputtering [26], molecular beam epitaxy [27], coreduction from solution [22], and so on. However, doping at the nanoscale, especially with ultrahigh concentration, remains both a formidable challenge and a tremendous opportunity [28].

Herein we present the synthesis of P-doped Na_4Si_4, using a reaction route similar to that reported to prepare the Zintl salt Na_4Si_4 [29,30]. The successfully doped Na_4Si_4 phase could be an important precursor to the correspondingly doped clathrate phases or Si NPs. A series of samples with P attempting to replace 1, 2, and 3 at% Si were investigated and the products were characterized by X-ray powder diffraction, energy dispersive X-ray (EDX) spectroscopy, Fourier-transform (FT) Raman, ^{29}Si, ^{23}Na, and ^{31}P solid-state magic-angle-spinning nuclear magnetic

* Corresponding author.
E-mail address: smkauzlarich@ucdavis.edu (S.M. Kauzlarich).

0022-4596/$ - see front matter © 2010 Elsevier Inc. All rights reserved.
doi:10.1016/j.jssc.2010.07.051

resonance (MAS NMR) spectroscopic techniques. The results show that P was successfully doped into Na_4Si_4 and the remaining P is transformed to black phosphorus.

2. Experimental

2.1. Synthesis

The materials used are Na lump (99%, Sigma-Aldrich), Si (99.99999+% lump from Johnson Matthey (JM), ball-milled to fine powder), P (red polycrystalline powder, JM grade A1A). For the synthesis of $Na_4Si_{4-x}P_x$ series, x values were chosen as 0.04, 0.08, and 0.12. The P concentrations, i.e. the ratios of P atoms to the sum of P and Si atoms, are 1, 2, and 3 at%, respectively. Si and P powder mixtures of 99:1, 98:2, and 97:3 in molar ratios were ball-milled for 30 min with Spex SamplePrep 8000 M Mixer/Mill. The Si:P mixtures with a slight excess of Na to form $Na_4Si_{4-x}P_x$ were loaded in niobium (Nb) tubes, which were sealed with an argon arc welder and subsequently contained in evacuated and sealed quartz ampoules. The reactions were carried out at 650 °C for 72 hours. Pristine Na_4Si_4 was also prepared by this method. The resulting products are black powders, which are air and moisture sensitive and therefore were handled and stored in N_2 filled glove box. All compositions have been characterized by powder X-ray diffraction. All peaks in all samples are found to be in good agreement with the diffraction pattern characteristic of Na_4Si_4. Most samples showed additional intensity could be assigned to the 100% peak for Na [31], and occasionally showed an additional peak that could be assigned to the 100% peak for NaOH [32], consistent with the ^{23}Na NMR results (see below).

2.2. Powder X-ray diffraction

Powder XRD experiments were run on a Bruker D8 Advance X-ray diffractometer (Cu $K\alpha_1$ radiation, $\lambda = 1.5406$ Å). The samples were sealed in a Bruker air-tight plastic sample holder prior to the experiments. Data sets were collected by DIFFRAC^{plus} XRD Commander program in a continuous scan mode between 10° and 80° in 2θ, with step size 0.021° and measuring time 2 s per step. Data were analyzed with MDI Jade Plus 6.1.1 software. Cell parameters were determined by the whole profile fitting (WPF) and refinement program available within the MDI Jade suite of programs. The two agreement factors, weighted (R) and the expected (E), are defined by the following equations: $R = 100 \times [\sum(w(i) \times (I(o,i) - I(c,i))^2) / \sum(w(i) - (I(o,i) - I(b,i)^2)]^{1/2}$ and $E = 100 \times [(N-P)/\sum I(o,i)]^{1/2}$, where $I(o,i)$ is the observed intensity of a fitted data point (i), $I(c,i)$ is the calculated intensity at this data point, $I(b,i)$ is the background intensity at this data point, $w(i)$ is the statistical weight of this data point, N is the number of the fitted data point, P is the number of refined parameters, and the sum is over all the fitted data points (N) that are 2σ above the fitted background. The ratio of R/E is called the "goodness of fit", which would be 1 in an ideal refinement. The calculated pattern of Na_4Si_4 was obtained by using CrystalMaker 7.2.3 software and the Na_4Si_4 unit cell data [30]. The WPF with experimental, calculated and difference plots are provided as Supporting Information.

2.3. EDX

The EDX spectra were obtained by the EDAX EDX system attached to the FEI/Philips XL30- SFEG scanning electron microscope. All samples weighed 3.0–3.5 mg; each was pressed into a small pellet and then mounted via double sticking carbon tape onto an aluminum stud. There was a few seconds exposure in the air when the aluminum studs were transferred into the vacuum chamber of the microscope. For each sample, 8–10 spots were chosen for observation in a random but consistent fashion to make sure that a survey of data points were collected that were representative of the sample. The acceleration voltage was 5 keV, all SEM images were taken at 10,000 × magnification, working distance of lens was about 5 mm and the acquisition time for all EDX spectra was 64 s.

2.4. Raman spectroscopy

FT Raman spectra were collected on samples taken in sealed thin quartz capillaries using a Bruker RFS 100/S Fourier-transform (FT) Raman spectrometer. Samples were irradiated with a frequency-doubled Nd:YAG laser operating at a wavelength of 1064 nm. The scattering signal was collected using a 180° backscattering geometry. The spectral resolution of the solid-state Ge detector was set to 1 cm^{-1}. A laser power level of 250 mW was used for all samples and approximately 6000 scans were collected at room temperature.

2.5. NMR spectroscopy

All solid-state ^{23}Na, ^{29}Si, and ^{31}P MAS NMR experiments were conducted on a Bruker Avance NMR spectrometer equipped with an 11.7 T wide-bore magnet. A Bruker 4 mm CPMAS probe was used with zirconia rotors and kel-F caps. The solid powder samples were loaded in the rotor inside a glove box filled with flowing nitrogen gas. Samples were spun at a rate of 15 kHz for the MAS NMR experiments. The ^{31}P MAS NMR spectra were recorded with direct polarization pulse sequence, with a 2.4 μs pulse (corresponding to 60° tip angle) and 30 s recycle delay. A total of 80–2000 transients were averaged and Fourier transformed with 200 Hz line broadening to obtain each spectrum. The chemical shifts were externally referenced to 85% H_3PO_4. The ^{29}Si MAS NMR spectra were recorded with direct polarization pulse sequence, with a 2 μs pulse (corresponding to 60° tip angle) and 500 s recycle delay; 200–800 transients were averaged and Fourier transformed with 100 Hz line broadening to obtain each spectrum. The ^{29}Si chemical shifts were externally referenced to $Si(CH_3)_4$. ^{23}Na MAS NMR spectra of these samples were recorded with direct polarization pulse sequence, with a pulse length of 0.25 μs (15° solids tip angle) and a recycle delay of 0.2 s. 2000 transients were averaged and Fourier transformed with 1 Hz line broadening to obtain each spectrum. The ^{23}Na chemical shifts were externally referenced to 1 M NaCl solution.

3. Results and discussion

The crystal structure of Na_4Si_4 has been described in detail previously [29,30], however, a brief description here is helpful for discussion of the Raman and solid-state NMR results obtained in this study. Na_4Si_4 crystallizes in a monoclinic structure with two crystallographically inequivalent sites for Si and Na: Si1 and Si2, Na1 and Na2. The structure with atom designation is shown in Fig. 1. The Zintl anion Si_4^{4-} forms a covalently bonded, distorted tetrahedron with four edge lengths slightly different from each other. The faces of the tetrahedron, composed of Si2–Si2–Si1 and Si1–Si1–Si2 are μ3 capped by Na1 and Na2, respectively, with slightly different average distances from the face center [30]. The Si1–Si2 edges are μ2 bridged by Na1; however, neither the Si1–Si1 nor the Si2–Si2 edges are coordinated by Na. The Si1 sites are μ1 contacted by both Na1 and Na2, with slightly different distances, while the Si2 sites have two μ1 contacts to Na2 [30].

The contacts of Na atoms with the tetrahedron are indicated in Fig. 1.

Table 1 provides the lattice parameters of the $Na_4Si_{4-x}P_x$ series. The cell parameters of the pristine Na_4Si_4 agree with the literature [30] and the refinements provide good R values (WPF provided in Supporting Information). As P content increases, the lattice parameters systematically increase. Since P is smaller than Si, this suggests that more complex interactions in the structure are important here, such as Na···P interactions and the distortion of the Si_4^{4-} tetrahedron.

Fig. 2 provides the calculated and experimental X-ray diffraction patterns of Na_4Si_4. The experimental pattern for Na_4Si_4 shows good agreement with the calculated pattern; there is one peak with additional intensity that is coincident with the 100% peak for Na [31], and an additional small peak that is consistent with the 100% peak for NaOH [32]. Both of these peaks varied in height from sample to sample and the one attributed to NaOH grew in intensity with time due to exposure of the sample to trace amounts of air, providing additional validity to the assignments. The powder XRD patterns for the $Na_4Si_{4-x}P_x$ series are provided in Fig. 3 corresponding to the atomic % of P in the Zintl Si_4^{4-} anion of 1%, 2%, and 3%, respectively. The samples will be referred to hereafter according to the atomic %. In this figure, the 2% and 3% samples show a peak that is attributed to NaOH, although all spectra show additional intensity for the peak indicated as Na 100% peak in Fig. 2. The maximum solid solubility of P in Si is approximately 2.4 at% at 1180 °C [33,34] and since P_4 and Si_4^{4-} are isoelectronic, the amount that was investigated was limited to 3%. The diffraction patterns of the P containing samples correspond well to the Na_4Si_4 structure, however close examination shows a couple of intensity changes with the most notable change being the growth of a new peak at approximately $2\theta=34.5^\circ$ which increases with increasing P in Fig. 3. The WPF, which does not subtract the background of the air-sensitive holder, is provided as Supporting Information and shows that this peak increase from 1 to 3 at%. This peak can be assigned to the 100% peak for orthorhombic black phosphorus with lattice parameters of $a=3.365$, $b=10.534$, $c=4.429$ Å, slightly larger than those reported ($a=3.3164$ (5), $b=10.484$ (3), $c=4.3793$ (5) Å) [33,34].

Black phosphorus is not easily prepared requiring a flux, catalyst or high pressure. Recently two routes for the conversion of red to black phosphorus have been reported: a low-pressure route using a mineralizer as a reaction promoter [35] and high energy mechanical milling [33,34]. The diffraction results for phosphorus doping of Na_4Si_4 suggest that at about 1 at%, some of the additional phosphorus is converted to orthorhombic black phosphorus with slightly larger lattice parameters than that reported [35]. There may be advantages to the presence of black phosphorus with metal silicide Zintl salts, for example: black phosphorus has been recently investigated as an electrode material for rechargeable lithium-ion batteries [36] and therefore it may be reasonable to pursue this route with Li–Si Zintl salts to further optimize their battery performance [36,37]. EDX experiments provided values of 0.9 (5), 1.8 (6), 2.6 (7) P at% for the prepared 1, 2, and 3 at% samples indicating that P is present in all cases, consistent with the amounts introduced in the synthesis. Raman and solid-state NMR spectroscopies allow specific investigation of the Na_4Si_4 structure, even in the presence of the additional black phosphorus phase. Both Raman spectroscopy and solid-state NMR are local probes and can distinguish phosphorus in the Na_4Si_4 lattice from black phosphorus.

The Raman spectra of Na_4Si_4 and the three doped samples are shown in Fig. 4. The Raman spectrum of Na_4Si_4 is in good

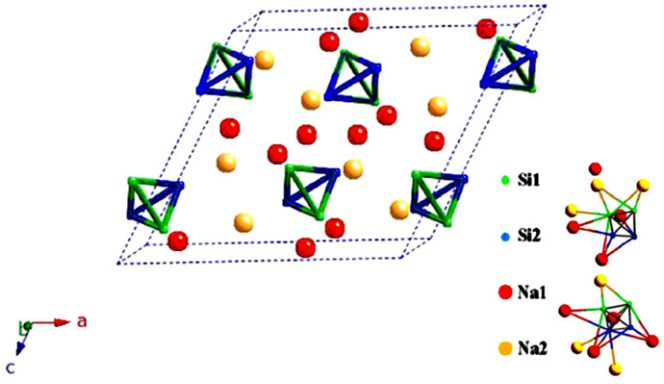

Fig. 1. A view of the monoclinic crystal structure of Na_4Si_4, along with the contacts for Na and Si indicated, drawn with CrystalMaker 7.2.3. software. Unit cell parameters used are: $a=12.1536$ Å, $b=6.5452$ Å, $c=11.1323$ Å, and $\beta=118.9^\circ$ (Ref. [30]).

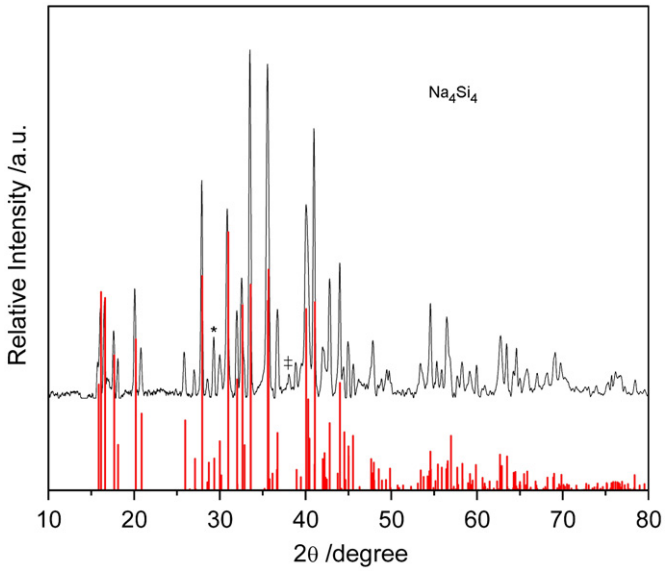

Fig. 2. Experimental X-ray powder diffraction pattern of Na_4Si_4 (black solid line) compared with the calculated pattern. A slight excess of Na provides additional intensity for the peak indicated by * and the 100% intensity peak for NaOH is indicated by ‡.

Table 1
Cell parameters of the $Na_4Si_{4-x}P_x$: $x=0.04$ (1 at%), 0.08 (2 at%), and 0.12 (3 at%).

	a (Å)	b (Å)	c (Å)	β (deg.)	V (Å^3)	R (%)	E (%)	R/E ratio
1 at%	12.173 (4)	6.554 (4)	11.147 (4)	118.95 (1)	778.2 (6)	3.00	0.69	4.3
2 at%	12.180 (8)	6.559 (8)	11.152 (8)	118.99 (2)	779 (1)	3.54	0.70	5.1
3 at%	12.180 (9)	6.561 (9)	11.154 (8)	118.96 (2)	780 (1)	4.22	0.71	5.9
Na_4Si_4 (as prepared)[a]	12.168 (2)	6.551 (2)	11.146 (2)	118.94 (1)	777.5 (3)	3.46	0.79	4.4
Na_4Si_4 (Ref. [30])	12.1536 (5)	6.5452 (5)	11.1323 (6)	118.9 (1)	775.3 (1)			

[a] Average values are shown here based on three different batches of Na_4Si_4 products as prepared.

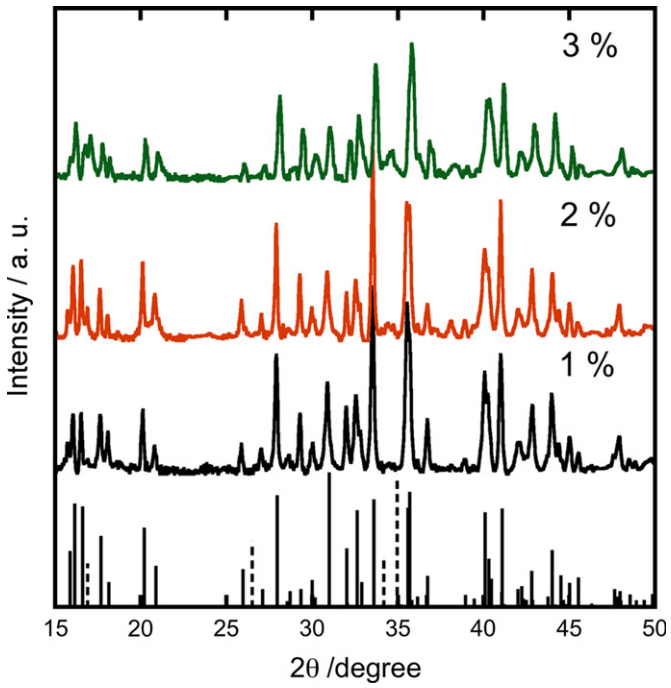

Fig. 3. Experimental X-ray powder diffraction pattern of the $Na_4Si_{4-x}P_x$ series: $x=0.04$ (1 at%); $x=0.08$ (2 at%), and $x=0.12$ (3 at%). The calculated diffraction pattern for Na_4Si_4 is provided. The peaks corresponding to black phosphorus [33] are indicated by dotted lines.

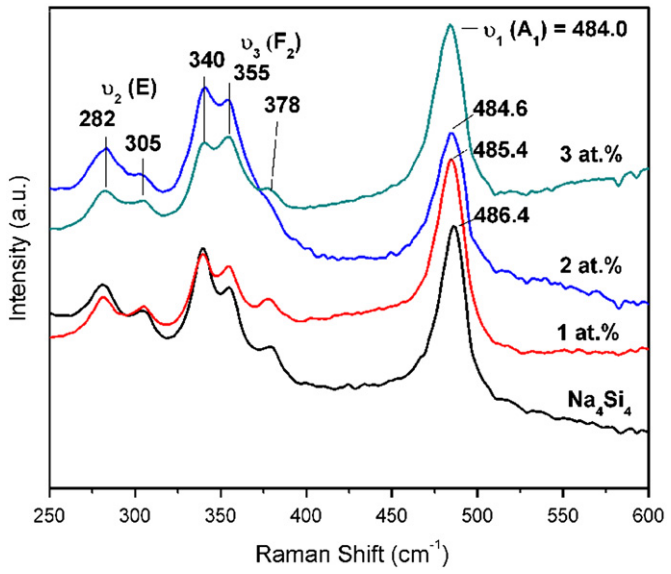

Fig. 4. Raman spectra of the $Na_4Si_{4-x}P_x$ series: $x=0.04$ (1 at%); $x=0.08$ (2 at%), and $x=0.12$ (3 at%), in comparison with pristine Na_4Si_4.

agreement with literature [38]. Three vibrational modes are expected for a perfect tetrahedral Si_4^{4-} cluster with T_d symmetry: the non-degenerate $v_1(A_1)$ "breathing" mode, the doubly degenerate $v_2(E)$ and the triply degenerate $v_3(F_2)$ mode. The distorted nature of the tetrahedral Si_4^{4-} cluster in Na_4Si_4 as well as the interaction with the Na^+ cation lifts such degeneracy and all six vibrational modes expected from a cluster of 4 Si atoms are distinctly observed in the FT Raman spectrum of Na_4Si_4. The Raman shift at 486.4 cm^{-1} can be assigned to the $v_1(A_1)$ mode of the Si_4^{4-} cluster, while the doublet (282, 305 cm^{-1}) and the triplet (340, 355, 378 cm^{-1}) bands can be assigned to the v_2 (E) and the v_3 (F_2) modes, respectively [38]. The Raman spectra for the 1, 2, and 3 at% P-doped samples show v_1 values of 485.4, 484.6, and 484.0 cm^{-1}, respectively, with an appreciable and monotonic trend of decreasing v_1, consistent with the weaker valence force constant and the larger reduced mass as the P concentration increases.

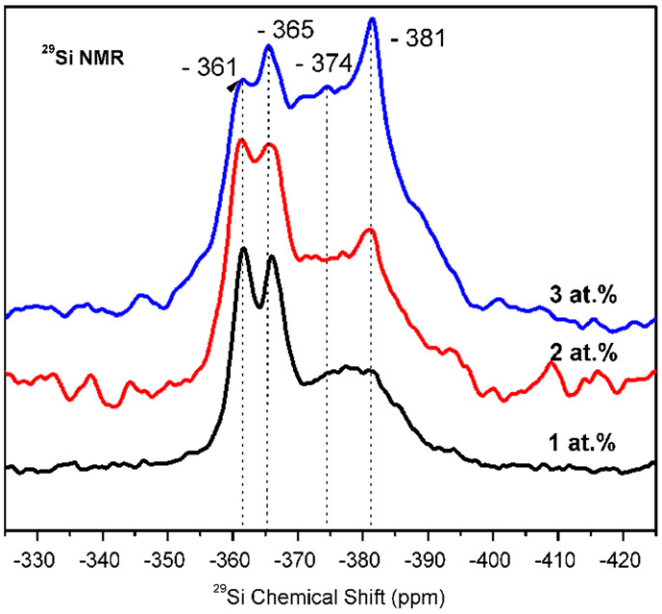

Fig. 5. ^{29}Si MAS NMR spectra for $Na_4Si_{4-x}P_x$ series: $x=0.04$ (1 at%); $x=0.08$ (2 at%); $x=0.12$ (3 at%).

Solid-state MAS NMR spectroscopy is a powerful tool to obtain local structural information of inter-atomic bonding and coordination environments and provides complementary information to XRD. Fig. 5 shows the ^{29}Si MAS NMR spectra of the 1, 2, and 3 at% P-doped Na_4Si_4 samples. The two relatively sharp resonances present in all spectra at -361 and -365 ppm correspond to the two crystallographically non-equivalent Si sites in pristine Na_4Si_4 lattice [10]. An additional distinct resonance signal at -381 ppm, together with at least one shoulder signal at -374 ppm, can be assigned to the Si sites in the Si_4 tetrahedra where one or more Si atom has been replaced by P due to doping. Since P has one more electron than Si donating to the tetrahedron, it provides more shielding to the Si nuclides, thus shifting this peak slightly upfield compared to those characteristic of pristine Na_4Si_4. It should be noted that for typical Si–P distances on the order of 0.25 nm in a P-substituted Si_4 tetrahedron, the ^{29}Si-^{31}P dipolar coupling constant can be calculated to be $\sim$600 Hz. Therefore, for MAS at 15 kHz, such interaction should be averaged in the ^{29}Si NMR spectra shown in Fig. 5. The broad line width of the resonance between -371 and -381 ppm may represent heterogeneous broadening due to local structural disorder resulting from P substitution in the lattice. In addition, it may be attributed to homogeneous broadening due to dipolar coupling with free electron resulting from n-type doping. In either case, it provides strong evidence for the substitution of P in the Si_4^{4-} cluster. This resonance at -381 ppm grows and sharpens as the P concentration increases from 1 to 3 at%, indicating an increasing fraction of P-substituted Si_4 tetrahedra. However, precise amounts cannot be quantified due to differential spin-lattice relaxation rates of Si nuclides in different environments. The peaks at -361 and -365 ppm belonging to the majority of the Si sites in the non-doped environment show much lower relative intensity in all spectra than they should due to the incomplete relaxation of these sites resulting from their long spin-lattice (T_1) relaxation times. On the other hand, the Si sites in the P-substituted tetrahedra are

able to relax much faster resulting in disproportionally high intensity, which should not be confused with their actual concentration. This fact is further demonstrated in Fig. 6, in which are shown the ^{29}Si NMR spectra for the 3 at% sample collected with recycle delay times of 100 and 500 s, respectively. The relatively higher intensity of the peaks corresponding to Si sites in the non-doped tetrahedron in the spectrum collected with longer recycle delay implies that these sites have a significantly longer T_1 than the Si sites in P-substituted Si_4 tetrahedra.

Fig. 7 shows the ^{23}Na MAS NMR spectra for the 1, 2, and 3 at% samples. The two Na sites in pristine Na_4Si_4 have been characterized by isotropic chemical shifts δ_{iso} of 56.7 and 49.5 ppm and corresponding quadrupolar coupling constants C_q of 1.25 and 2.31 MHz and asymmetry parameters η of 1.0 and 0.15, respectively [10]. As expected, these two sites are also present in nearly equal proportions the ^{23}Na MAS NMR spectra for the 1, 2, and 3 at% samples (Figs. 7 and 8). In addition to these two sites (Fig. 8), the presence of a third site with a δ_{iso} of 53.3 ppm and with C_q and η of 2.0 MHz and 0.10, respectively is indicated by constrained line shape simulation of these spectra. This new site can be attributed to Na atoms neighboring P-substituted Si_4 tetrahedra and its concentration does not change appreciably with P concentration. The relative fractions of this Na site are 25 (3)%, 23 (3)%, and 26 (3)%, respectively, for the 1, 2, and 3 at%

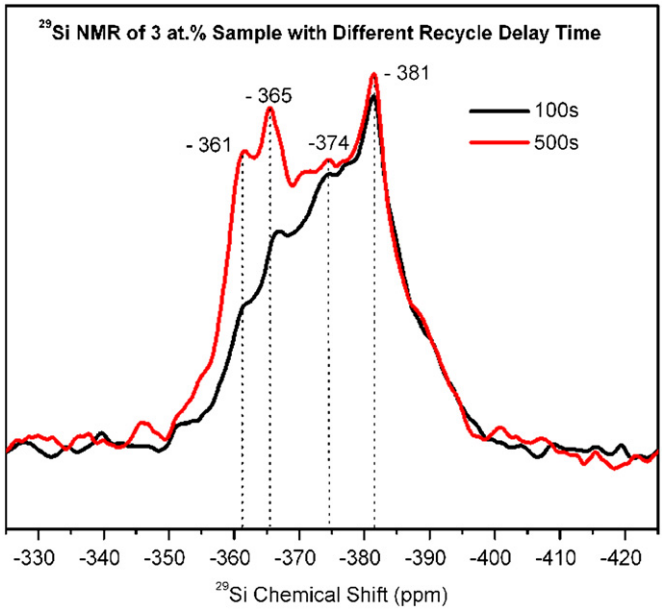

Fig. 6. ^{29}Si MAS NMR spectra for 3 at% P-doped Na_4Si_4 sample with recycle delay times of 100 and 500 s.

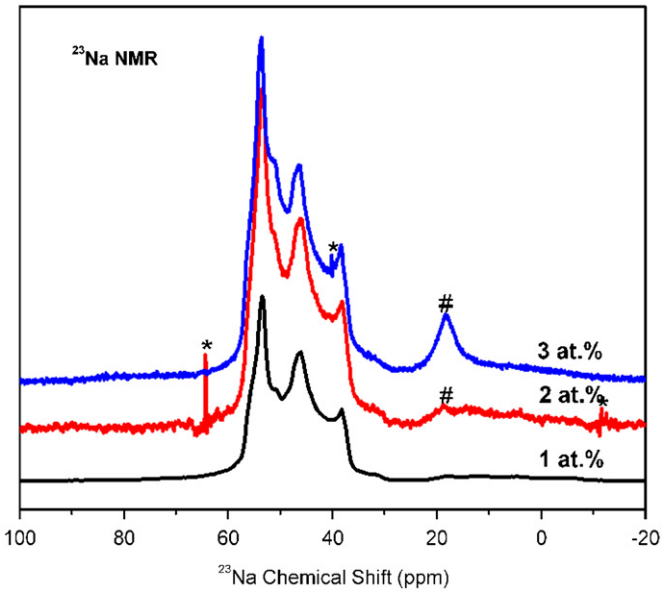

Fig. 7. ^{23}Na MAS NMR spectra for $Na_4Si_{4-x}P_x$ series: x=0.04 (1 at%); x=0.08 (2 at%); x=0.12 (3 at%). The peak marked with # sign is attributed to a small amount of NaOH impurity and the sharp spikes in the spectra denoted by asterisks correspond to probe arcing.

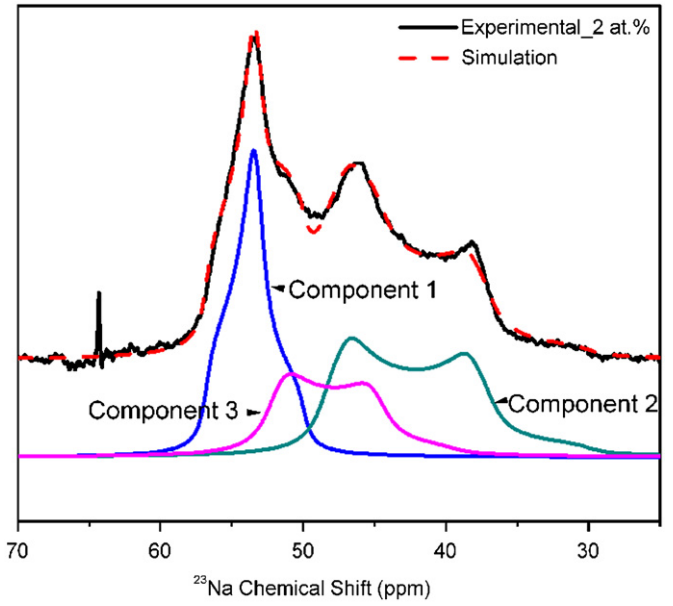

Fig. 8. The experimental (solid line) and simulated (dashed line) ^{23}Na MAS NMR spectra for the 2 at% P-doped Na_4Si_4 sample. The individual simulation components are vertically offset for the sake of clarity. Components 1 and 2 are present in nearly equal proportions and correspond to the two Na sites in the pristine Na_4Si_4. Component 3 is attributed to the Na atoms neighboring P-substituted Si tetrahedra.

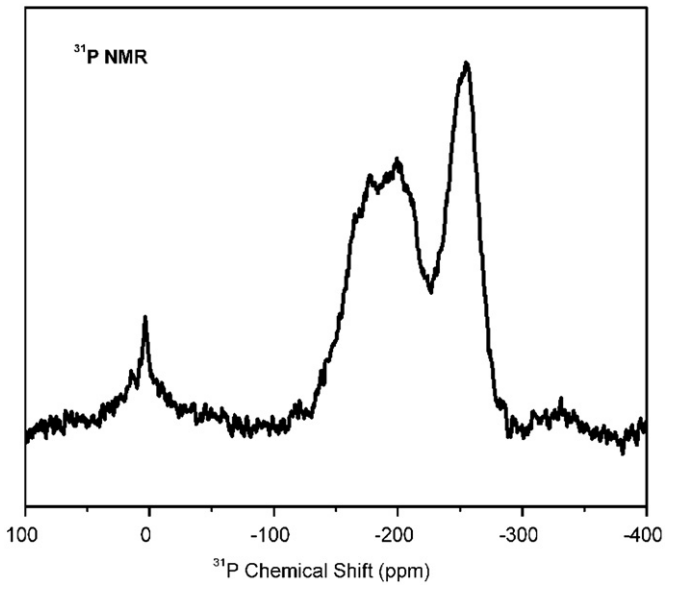

Fig. 9. ^{31}P MAS NMR spectrum for 1 at% P-doped Na_4Si_4 sample.

samples. The resonance signal marked with the # sign at 18.4 ppm is attributed to a small amount of NaOH impurity present in these samples.

Fig. 9 shows the ^{31}P NMR spectra of the 1 at% sample. There are two broad signals centered at around −190 and −260 ppm, corresponding to at least two crystallographically inequivalent sites for P substituting Si in the tetrahedral structure, consistent with the crystal structure for Na_4Si_4. The up field shift (negative value) with respect to the H_3PO_4 reference is consistent with the more shielded P–Si environment than the P–O environment. These two P sites are present at a ratio of 3:2 in this sample. Black phosphorus has a sharp resonance at 22.2 ppm and there is a split resonance at approximately 13 ppm in the ^{31}P NMR spectrum of the 1 at% sample. Similar to the powder diffraction results, this peak is shifted from the reported resonance for black phosphorus, suggesting that the phase is similar to but not identical to what has previously been reported [34].

4. Conclusions

In summary, the P-doped Zintl salt $Na_4Si_{4-x}P_x$ (x=0.04, 0.08, 0.12), corresponding to P concentrations in the Si tetrahedron of 1, 2, and 3 at%, have been investigated. The products were characterized by powder XRD, EDX, FT Raman, ^{23}Na, ^{29}Si and ^{31}P solid–state MAS NMR spectroscopy. The results show that the P-doping has been successfully achieved in the lattice of Na_4Si_4. As the amount of phosphorus increases from 1 to 3 at%, a new diffraction peak that is consistent with the presence of black phosphorus becomes apparent in the samples, suggesting that the maximum amount of dopant in Na_4Si_4 is less than 1 at%. The P-doped Na_4Si_4 synthesized in this work might be used as precursor to prepare corresponding P-doped Si NPs, P-doped Si clathrate phases and other materials where Na_4Si_4 has been shown to be an appropriate starting material. Additionally, the presence of black phosphorus may be advantageous for battery applications and a similar study is worth pursuing for the Li–Si Zintl phases that show promise for Li-ion batteries.

Acknowledgments

Financial support from the US DOE Center of Excellence for Chemical Hydrogen Storage and DOE grant DE-FG02-03ER46057 are gratefully acknowledged. The assistance of Tanghong Yi and Fen Xu with the X-ray diffraction analysis is gratefully acknowledged.

Appendix A. Supplementary material

Supplementary data associated with this article can be found in the online version at doi:10.1016/j.jssc.2010.07.051.

References

[1] L.J. Chen, Silicide Technology for Integrated Circuits. London: Institution of Electrical Engineers, 2004.
[2] X.C. Ma, F. Xu, T.M. Atkins, A.M. Goforth, D. Neiner, A. Navrotsky, S.M. Kauzlarich, Dalton Transactions (2009) 10250.
[3] C. Cros, M. Pouchard, E.P. Hagenmuller, Journal of Solid State Chemistry 2 (1970) 570.
[4] J.S. Kasper, P. Hagenmul, M. Pouchard, C. Cros, Science 150 (1965) 1713.
[5] D. Neiner, N.L. Okamoto, C.L. Condron, Q.M. Ramasse, P. Yu, N.D. Browning, S.M. Kauzlarich, Journal of the American Chemical Society 129 (2007) 13857.
[6] H.-o. Horie, T. Kikudome, K. Teramura, S. Yamanaka, Journal of Solid State Chemistry 182 (2009) 129.
[7] G.S. Nolas, J.L. Cohn, G.A. Slack, S.B. Schujman, Applied Physics Letters 73 (1998) 178.
[8] M. Beekman, G.S. Nolas, Journal of Materials Chemistry 18 (2008) 842.
[9] J. Gryko, P.F. McMillan, R.F. Marzke, G.K. Ramachandran, D. Patton, S.K. Deb, O.F. Sankey, Phys. Rev. B 62 (2000) R7707.
[10] D. Mayeri, B.L. Phillips, M.P. Augustine, S.M. Kauzlarich, Chemistry of Materials 13 (2001) 765.
[11] P.F. McMillan, J. Grykoc, C. Bulld, R. Arledgec, A.J. Kenyone, B.A. Cressey, Journal of Solid State Chemistry 178 (2005) 937.
[12] D. Neiner, H.W. Chiu, S.M. Kauzlarich, Journal of the American Chemical Society 128 (2006) 11016.
[13] D. Neiner, S.M. Kauzlarich, Chemistry of Materials 22 (2010) 487.
[14] S. Lee, W.J. Cho, C.S. Chin, I.K. Han, W.J. Choi, Y.J. Park, J.D. Song, J.I. Lee, Japanese Journal of Applied Physics Part 2—Letters & Express Letters 43 (2004) L784.
[15] J.I. Tani, H. Kido, Intermetallics 16 (2008) 418.
[16] S. Kuroiwa, H. Kawashima, H. Kinoshita, H. Okabe, J. Akimitsu, Physica C—Superconductivity and its Applications 466 (2007) 11.
[17] A. Mimura, M. Fujii, S. Hayashi, D. Kovalev, F. Koch, Physical Review B 62 (2000) 12625.
[18] X.D. Pi, R. Gresback, R.W. Liptak, S.A. Campbell, U. Kortshagen, Applied Physics Letters 92 (2008) 123102.
[19] Y. Ono, J.F. Morizur, K. Nishiguchi, K. Takashina, H. Yamaguchi, K. Hiratsuka, S. Horiguchi, H. Inokawa, Y. Takahashi, Physical Review B 74 (2006) 235317.
[20] Y. Matsumoto, Z.R. Yu, Japanese Journal of Applied Physics Part 1—Regular Papers Short Notes & Review Papers 40 (2001) 2110.
[21] T. Itoh, Y. Katoh, T. Fujiwara, K. Fukunaga, S. Nonomura, S. Nitta, Thin Solid Films 395 (2001) 240.
[22] R.K. Baldwin, J. Zou, K.A. Pettigrew, G.J. Yeagle, R.D. Britt, S.M. Kauzlarich, Chemical Communications (2006) 658.
[23] X. Zhang, M. Brynda, R.D. Britt, E.C. Carroll, D.S. Larsen, A.Y. Louie, S.M. Kauzlarich, Journal of the American Chemical Society 129 (2007) 10668.
[24] W.S. Wei, G.Y. Xu, J.L. Wang, T.M. Wang, Vacuum 81 (2007) 656.
[25] J. Chen, J.P. Colinge, D. Flandre, R. Gillon, J.P. Raskin, D. Vanhoenacker, Journal of the Electrochemical Society 144 (1997) 2437.
[26] Y. Ohmura, M. Takahashi, M. Suzuki, A. Emura, N. Sakamoto, T. Meguro, Y. Yamamoto, Physica Status Solidi B—Basic Research 235 (2003) 111.
[27] M. Miyao; K. Nakagawa, Japanese Journal of Applied Physics Part 1—Regular Papers Short Notes & Review Papers 33 (1994) 3791.
[28] D.J. Norris, A.L. Efros, S.C. Erwin, Science 319 (2008) 1776.
[29] J. Witte, H.G. von Schnering, Zeitschrift fur Anorganische und Allgemeine Chemie 327 (1964) 260.
[30] T. Goebel, Y. Prots, F. Haarmann, Zeitschrift Fur Kristallographie—New Crystal Structures 223 (2008) 187.
[31] C.S. Barrett, Acta Crystallographica 9 (1956) 671.
[32] H. Jacobs, J. Kockelkorn, T. Tacke, Zeitschrift Fur Anorganische Und Allgemeine Chemie 531 (1985) 119.
[33] S. Lange, P. Schmidt, T. Nilges, Inorganic Chemistry 46 (2007) 4028.
[34] T. Nilges, M. Kersting, T. Pfeifer, Journal of Solid State Chemistry 181 (2008) 1707.
[35] C.-M. Park, H.-J. Sohn, Advanced Materials 19 (2007) 2465.
[36] Y. Yang, M.T. McDowell, A. Jackson, J.J. Cha, S.S. Hong, Y. Cui, Nano Letters 10 (2010) 1486.
[37] C.K. Chan, H. Peng, G. Liu, K. McIlwrath, X.F. Zhang, R.A. Huggins, Y. Cui, Nature Nanotechnology (2008) 31.
[38] M. Somer, Zeitschrift Fur Anorganische Und, Allgemeine Chemie 626 (2000) 2478.